# Round trip times versus the range of the radargram maxima of an air-coupled bistatic GPR: Modeling and fitting by a hyperbola

Christophe Bourlier

# Round trip times versus the range of the radargram maxima of an air-coupled bistatic GPR: Modeling and fitting by a hyperbola

Christophe Bourlier

***Abstract*—For a circular cylinder in free space and for a monostatic configuration (transmitter and receiver are identical), from a geometrical way, it is well-known that the maxima of the GPR (ground penetrating radar) rardargram (or B-scan) cross section follows a hyperbola profile $t = w(x_2)$ (time $t$ versus the receiver range $x_2$). For a buried object and for a coupled-air monostatic configuration, this statement is no longer valid. The purpose of this letter is to generalize the derivation of $w$ to a bistatic (transmitter and receiver are distinct) configuration by investigating two approaches based on a geometrical way: The conventional mid-point approximation technique and a new more physical way based on the specular direction. In addition, a study is led on the fitting of $w$ by a hyperbola and a polynomial function of fourth degree. The resulting closed-form expressions are compared with the results obtained from the full-wave method of moments to verify their accuracy.**

***Index Terms*—Ground-penetrating radar, electromagnetic propagation, B-scan, hyperbola, specular reflection.**

## I. Introduction

Ground-penetrating radar (GPR) is an efficient tool, applied in a wide range of applications, in order to provide a qualitative information on the auscultated medium. Its principle is based on the study of the time-range echoes both produced by the top interface and buried objects. By solving the inversion problem, their features can be determined with uncertainties. Due to the antenna radiation pattern, it is well known that local objects (various types of pipes, rebars, tree roots, etc.) present a particular hyperbolic-shaped signature in the GPR radargram cross section. More precisely, for a given range $x_2$ of the receiver, the location of the time points for which the radargram (or B-scan, i. e., scattered electromagnetic field measured by the receiver versus the range-time $(x_2, t)$) is maximum, follows a curve of equation $t = w(x_2)$, where $w$ is assumed to be a hyperbola function.

In recent years, it was shown that inversion algorithms, like deep learning based-tools, can automatically detect the $w$ profile in radargrams using data measured over urban infrastructure or archaeological dataset with diverse underground structures [1], [2], [3], [4], [5], [6], [7]. These algorithms need to solve the forward problem, that is to model the function $w$. For the monostatic case (transmitter and receiver locations are the same) and by considering a circular cylinder in free space (or ground-coupled configuration), strictly speaking, $w$ is a hyperbola function [1], [3], [5]. On the other hand, for a bistatic (transmitter and receiver locations differ) configuration [2], [4], [6], [7], $w$ does not match with a hyperbola. Simply though, the term hyperbola is always used. For air-coupled monostatic data and for a circular cylinder buried in homogeneous medium, the derivation of $w$ is not straight-forward [8]. It requires to solve an equation of fourth degree. For ground-coupled data, it is important to underline that the propagation delay in free space is negligible. The formulation addresses in free space can be applied by replacing the light speed by that in the medium.

The first purpose of this letter is to generalize the derivation of $w$ to the air-coupled bistatic case and from two geometrical ways. The first one (named method M1), applied in all cited articles, assumes that the ray reflected by the cylinder is defined at the mid-abscissa between the emitter and receiver. The second one (named method M2), never published to our knowledge, is based on more physical considerations that this abscissa is obtained from the specular reflection on the cylinder. In addition, a study is led on the fitting of $w$, especially by a hyperbola and a polynomial function of fourth degree. The resulting closed-form expressions are compared with the results obtained from the full-wave method of moments (MoM) [9], [10].

The paper is organized as follows. Sections II addresses the derivations of $w$ for a buried circular cylinder by considering a coupled-air bistatic configuration. Section III compares them with the MoM and a study is led to fit the function $w$. The last section gives concluding remarks.

## II. Time delay for a buried object

In this section, the function $w$ is derived by considering a buried cylinder assumed to be circular, which means that the cross section of a pipe is illuminated in its orthogonal direction. First, the monostatic case is addressed (Fig. 1) and next, the bistatic configuration from the conventional method, named "M1" (in Fig. 2, the point $A$ is considered) and from the method based on the specular direction, named "M2" (in Fig. 2, the point $B$ is considered). The last section approximates $w$ by a hyperbola.

### A. Monostatic case

We consider the geometric shown in Fig. 1. A transmitter $T_x$ of coordinates $(x_1 = x, z_1 = z)$ emitting an incident electromagnetic wave and a receiver of same coordinates

C. Bourlier is with IETR (Institut d'Electronique et des Technologies numéRiques) laboratory, UMR CNRS 6164, Nantes Université, polytech Nantes, La Chantrerie, Nantes, France.

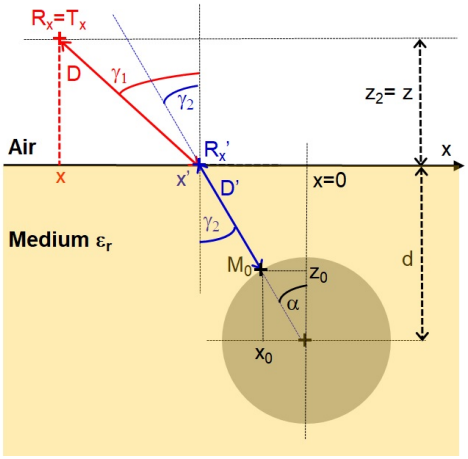


Fig. 1. Monostatic case of a buried object of depth $d$. The receiver $R_x$ and transmitter $T_x$ locations are identical, have coordinates $(x, z)$ and they are in free space. $M_0$ is a point belonging to the buried circular cylinder and $R'_x$ is a point of coordinates $(x', 0)$.

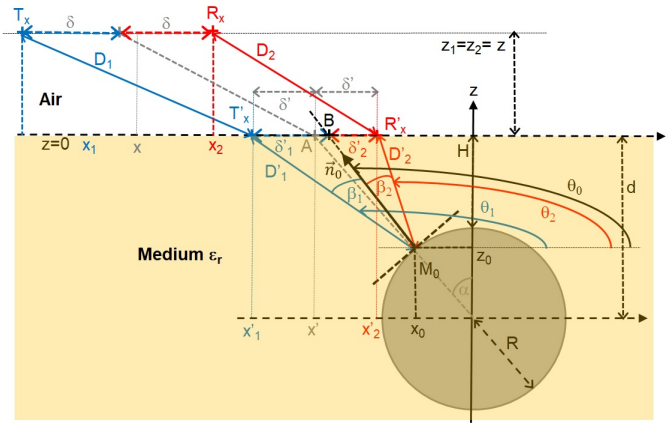


Fig. 2. Monostatic case of a buried object of depth $d$ and radius $R$. The point $T'_x$, has coordinates $(x'_1, z'_1 = 0)$ and $R'_x$ has coordinates $(x'_2, z'_2 = 0)$. For the conventional method, the point $A$ is located in the middle of the segment $[T'_x R'_x]$ ($\delta'_1 = \delta'_2 = \delta'$). For the method based on the "specular reflection", the point $B$ differs from $A$ and the distances $\delta'_1 \neq \delta'$ and $\delta'_2 \neq \delta'$ are defined. This method assumes that the angles $\beta_1 = \beta_2$.

$(x_2 = x, z_2 = z)$ (monostatic configuration) which measures the electromagnetic field scattered by the scene. For an object buried in the homogeneous medium of relative permittivity $\epsilon_r$, the time delay can be obtained from the time delay in free space, corresponding to the propagation from $R_x$ to the point $R'_x = (x', z = 0)$, plus the time delay in medium $\epsilon_r$, corresponding to the propagation from $R'_x$ to the point $M_0$ belonging to the buried object. For a round trip of the scattered wave, the total time delay is multiplied by two. Then

$$t = 2\left(D/c + D'/v\right), \tag{1}$$

$$\begin{cases} D = \sqrt{(x'-x)^2 + z^2},\ D' = \sqrt{(x_0 - x')^2 + (z_0 - d)^2} \\ x_0 = R\sin\alpha = Rx'/r,\ z_0 = R\cos\alpha = Rd/r \\ r = \sqrt{x'^2 + d^2} \end{cases}, \tag{2}$$

where $d > 0$ is the depth and $M_0$ a point of coordinates $(x_0, z_0)$ on the cylinder centered on $(0, -d)$. The abscissa $x'$ must be determined. From a Snell-Descartes law, $\sin\gamma_1 = \sqrt{\epsilon_r}\sin\gamma_2$. Since $\sin^2\gamma = 1/(1 + \cot^2\gamma)$, we have

$$\left(1 + \cot^2\gamma_1\right)^{-1} = \epsilon_r\left(1 + \cot^2\gamma_2\right)^{-1}, \tag{3}$$

where $\cot\gamma_1 = z/(x' - x)$ and $\cot\gamma_2 = -d/x'$. To find $x'$, from the above equation, the following equation of fourth degree must be solved

$$\begin{cases} c_0 + c_1 x' + c_2 x'^2 + c_3 x'^3 + c_4 x'^4 = 0 \\ c_0 = d^2 x^2,\ c_1 = -2d^2 x,\ c_2 = d^2 + x^2 - \epsilon_r(z^2 + x^2) \\ c_3 = 2x(\epsilon_r - 1),\ c_4 = 1 - \epsilon_r \end{cases}. \tag{4}$$

Persico et al. [8] derived the analytical solution of the above equation. In this paper, the unique physical solution is approximated, allowing us to obtain $w$ from a closed-from expression. The physical solution is real and for $x \leq 0$, $x' > x$ and for $x > 0$, $x' < x$. For $\epsilon_r = 1$, it is easy to show that $x' = xd/(z + d)$. To find an approximated solution of $x'$, we assume that $x' = cx$, where $c$ is independent of $x$. Reporting this expression in the first line of equation (4), we show that

$$x' \approx xd/\left(d + z\sqrt{\epsilon_r}\right). \tag{5}$$

### B. Bistatic case: Method 1

As shown in Fig. 2, for the bistatic case, $x_2 \neq x_1$ (but $z = z_1 = z_2$). The total time delay is

$$t = \frac{D_1 + D_2}{c} + \frac{D'_1 + D'_2}{v} = \frac{2}{v}\left(\frac{D_1 + D_2}{n} + D'_1 + D'_2\right), \tag{6}$$

where $n = \sqrt{\epsilon_r} = c/v$ (refraction index) and

$$\begin{cases} D_i = \sqrt{(x'_i - x_i)^2 + z^2} \\ D'_i = \sqrt{(x_0 - x'_i)^2 + (z_0 - d)^2} \end{cases}, \tag{7}$$

$$\begin{cases} x_0 = R\sin\alpha = Rx'/r,\ z_0 = R\cos\alpha = Rd/r \\ r = \sqrt{x'^2 + d^2},\ x' = (x'_1 + x'_2)/2 \end{cases}, \tag{8}$$

and $i = \{1, 2\}$. The abscissa $(x'_1, x'_2)$ are computed from equation (4) where $(x = x_1, x = x_2)$. Using equation (5), $(x'_1, x'_2)$ can be approximated as

$$x'_i \approx x_i d/\left(d + z\sqrt{\epsilon_r}\right). \tag{9}$$

As shown in Fig. 2, for the first method, it is important to underline that the abscissa $x$ is assumed to be defined as $(x_1 + x_2)/2$ ($x_{1,2} = x \mp \delta$).

### C. Bistatic case: Method 2

When an incident electromagnetic wave illuminates an object with a moderate curvature (to avoid the multiple reflection phenomenon) and with its smallest dimension greater than the electromagnetic wavelength, the scattered field mainly contributes in the specular direction. From Fig. 2, this direction occurs when $\beta_1 = \beta_2 = \beta$ and the scattered field can be computed from the tangent-plane or Kirchhoff approximations. $\beta_1$ and $\beta_2$ are the angles between the incident and receiver directions, respectively, and the normal $\hat{\boldsymbol{n}}_0$ to the slope at the point $M_0$. In all cited articles, the point $A$ is located in the middle of the segment $[T_x R_x]$ and in equation (8), $x' = (x'_1 + x'_2)/2$ . This statement is based on no physical

argument and implies that $\beta_1$ can differ from $\beta_2$: The point $B$ is different of $A$ and $\delta_1' \neq \delta_2' \neq \delta'$.

From Fig. 2, $\theta_0 = \theta_2 + \beta_2 = \theta_2 + \beta$ and $\theta_1 = \theta_2 + \beta_1 + \beta_2 = \theta_2 + 2\beta \Rightarrow \beta = (\theta_1 - \theta_2)/2$, where $\theta_2$ and $\theta_1$ are the polar angles giving the locations of the transmitter and receiver, respectively. Thus, $\theta_0 = \theta_2 + \beta = (\theta_1 + \theta_2)/2$ and the coordinates of the point $M_0$ are

$$\begin{cases} x_0 = R\cos\theta_0 = \pm R\sqrt{\left[1+\cos\left(\theta_1+\theta_2\right)\right]/2} \\ z_0 = R\sin\theta_0 \;\; = \;\; R\sqrt{\left[1-\cos\left(\theta_1+\theta_2\right)\right]/2} \end{cases}. \quad (10)$$

For $\theta_i \in [0;\pi]$ ($i = \{1,2\}$), $\theta_0 \in [0;\pi]$ and $z_0 \geq 0$. For $\theta_0 \in [0,\pi/2]$, $x_0 \geq 0$, otherwise $x_0 < 0$. Since $\tan\theta_i = z/x_i$, we can show

$$\begin{cases} \sqrt{2}x_0 = \pm R\sqrt{1+\left(x_1'x_2' - z^2\right)/\left(r_1 r_2\right)} \\ \sqrt{2}z_0 \;\; = \;\; R\sqrt{1-\left(x_1'x_2' - z^2\right)/\left(r_1 r_2\right)} \\ r_i = \sqrt{x_i'^2 + z^2} \end{cases}. \quad (11)$$

For method 2, equation (6) remains valid, but $(x_0, z_0)$ are computed from equation (11). For $x_1 = x_2 = x$, $r_1 = r_2 = r$ and equation (8) is found. For this special case, this means that $\delta_1 = \delta_2 = \delta$ and the time delay $t$ is the same for the two methods.

### *D. $w$ approximated by a hyperbola*

For a cylinder in free space, the time $t = 2(\sqrt{x^2+z^2} - R)/c$ where $z$ is the emitter-receiver height from the cylinder center. For this monostatic case, it is easy to show that the curve $t = w(x)$ is a hyperbola of apex coordinates $(0, 2[z - R]/c)$ and of slope $2/c$.

In equations (7), (8) and (11), due to the square roots in the variables $(D_i, D_i', r_i, r)$ and $(x_0, z_0)$ for M2, the function $w$ does not obey hyperbolic equation. For method 1 (named M1), to approximate the function $w$ governed by equation (6) by a hyperbola in the $(x,t)$ plane, $(D_i, D_i')$ are approximated by its Taylor's series expansion up to the orders $(2,2)$ over $(x,\delta)$ near $(0,0)$ as

$$\begin{cases} (D_1 + D_2)/n \approx a_0 + a_2 x^2 - R \\ (D_1' + D_2') \;\; \approx a_0' + a_2' x^2 - R \end{cases}, \quad (12)$$

where

$$\begin{cases} a_0 = R + \dfrac{z}{n}\left[2 + \dfrac{n^2\delta^2}{(nz+d)^2}\right] \qquad a_2 = \dfrac{zn}{(nz+d)^2} \\ a_0' = 2d - R + \dfrac{d^2\delta^2}{(d-R)(nz+d)^2} \;\; a_2' = \dfrac{d}{(nz+d)^2} \end{cases}. \quad (13)$$

In addition, reporting equation (12) into equation (6), we show

$$\left(t + \frac{2R}{v}\right)^2 \frac{1}{b^2} - \frac{x^2}{a^2} = 1, \quad (14)$$

where

$$a^2 = \left(a_0 + a_0'\right)/\left[2(a_2 + a_2')\right], \; b^2 = \left(a_0 + a_0'\right)^2/v^2. \quad (15)$$

Expression (14) is an equation of a hyperbola of apex coordinates $(-2R/v, -2R/v + b)$. For $\delta = 0$, $a_0 = R + 2z/n$, $a_0' = 2d - R$, $a_0 + a_0' = 2d + 2z/n$, $b = 2(d + z/n)/v$. Thus, $-2R/v + b = 2[(d-R)/v + z/c]$ corresponding to the round trip time from the top of the buried cylinder.

TABLE I
SIMULATION PARAMETERS OF SCENARIO $i$.

| $i$ | $z$ [cm] | $d$ [cm] | $R$ [cm] | $2\delta$ [cm] | $\epsilon_r$ |
|---|---|---|---|---|---|
| 1 | 50 | 40 | 10 | 10 | 4 |
| 2 | **5** | 40 | 10 | 10 | 4 |
| 3 | 50 | 40 | **20** | 10 | 4 |
| 4 | 50 | **20** | 10 | 10 | 4 |
| 5 | 50 | 40 | 10 | **30** | 4 |
| 6 | 50 | 40 | 10 | 10 | **2** |

TABLE II
HYPERBOLA PARAMETERS.

| $i$ | $x_0$ [cm] | $-t_0 + b$ [ns] | $b/a$ ns.cm$^{-1}$ | $\overline{\Delta_{x_0}}$, $\overline{\Delta_{z_0}}$ [cm] |
|---|---|---|---|---|
| 1 | 4.99-5.00 | 7.39-7.35 | 0.0825-0.0909 | 0.011, 0.001 |
| 2 | 4.94-5.00 | 4.42-4.37 | 0.1251-0.1234 | 0.092, 0.023 |
| 3 | 4.94-5.00 | 6.06-6.02 | 0.0821-0.0909 | 0.022, 0.003 |
| 4 | 4.99-5.00 | 4.72-4.68 | 0.0836-0.0818 | 0.015, 0.002 |
| 5 | 15.00-15.00 | 7.49-7.45 | 0.0855-0.0915 | 0.011, 001 |
| 6 | 4.96-5.00 | 6.22-6.17 | 0.0888-0.0778 | 0.024, 0.004 |

## III. NUMERICAL RESULTS

The input time signal is assumed to be a Ricker defined as

$$s(t) = \left(1 - 2\pi^2 f_0^2 t^2\right)\exp\left(-\pi^2 f_0^2 t^2\right), \quad (16)$$

where $f_0$ is the central frequency. In literature, $f_0$ can be changed by $f_0\sqrt{2}$. The Fourier transform of $s$ is

$$\hat{s}(f) = \int_{-\infty}^{+\infty} s(t)e^{-2\pi j f t}dt = \frac{2f^2}{\sqrt{\pi}f_0^3}\exp\left(-\frac{f^2}{f_0^2}\right). \quad (17)$$

We can note that $\hat{s}'(f) = 0$ if $f = \pm f_0$.

In the following, $f_0 = 2.5$ GHz and the frequency goes from $f_{\min} = 1.5$ GHz to $f_{\max} = 3.5$ GHz with a sampling step $\Delta f = 0.05$ GHz (41 frequencies). In the time domain, to calculate the A-scan, the sampling step is $\Delta t = 1/f_{\max}$ and the time goes from $t_{\min} = 0$ to $t_{\max} = N_{\text{IFFT}}\Delta t$ where $N_{\text{IFFT}} = 2^n$, with $n$ a positive integer, to apply the fast Fourier transform algorithm. In addition, to have a sampling step $\Delta t = 0.01$ ns, in the frequency domain, the padding technique is applied, which means that $\hat{s}(f) = 0$ for $f \notin [f_{\min}; f_{\max}]$.

The scattered field is computed from the boundary integral equations solved by the method of moments (MoM) addressed in [9]. First, for a single frequency and for given geometry and position of the transmitter $(x_1, z_1 = z)$, the currents are computed on the scatterer surfaces. They are performed by solving a linear system obtained by discretizing the boundary integral equations from the MoM. Next, for different positions of the receiver $(x_2, z_2 = z)$, the scattered field is computed from the radiation of the surface currents by applying the Huygens principle. For several frequencies, these two stages (current and radiation computations) are repeated to obtain $\hat{\Psi}_{\text{sca}}(x_2, f)$, the scattered field versus $x_2$ and $f$. To compute the B-scan, the IFFT is applied on the signal $\hat{\Psi}_{\text{sca}}(x_2, f)\hat{s}(f)$ where $\hat{s}(f)$ is defined by equation (17).

The incident field is the Hankel function (of zeroth order and of first kind) defined as $\psi_{\text{inc}}(\boldsymbol{r}_1, \boldsymbol{r}_0) = (j/4)\text{H}_0^{(1)}(k_0\left\|\boldsymbol{r}_0 - \boldsymbol{r}_1\right\|)$ modeling a source point radiation in near field, where $\boldsymbol{r}_0 = (x_0, z_0)$ are the coordinates of

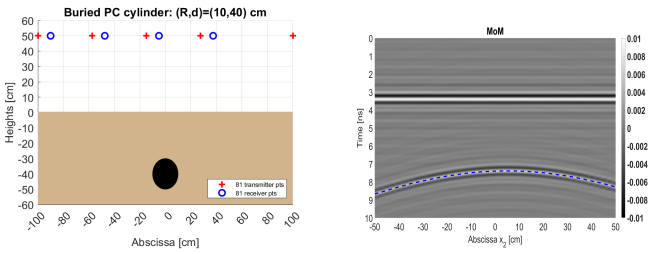


Fig. 3. On the left: Scenario 1; a buried metallic circular cylinder. The simulation parameters are listed in Table I where $i = 1$. On the right: Scattered field measured by the receiver versus $x_2$ and the time $t$ (B-scan). The blue-dashed curve plots the points for which the strength (related to the cylinder contribution) is maximum for a given $x_2$.

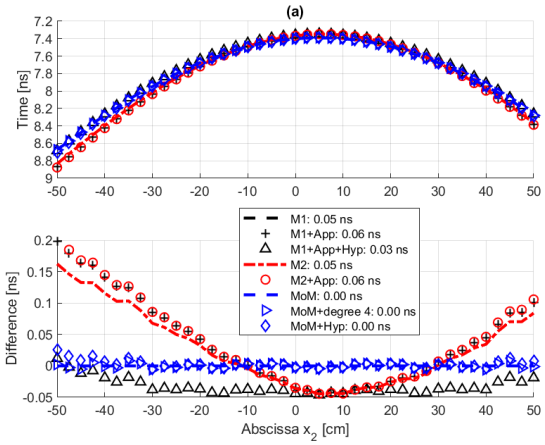


Fig. 4. Top: Time $T_{\max}$ giving the maximum of the scattered field versus $x_2$. The blue curve is the same as plotted on the left of Fig. 3. Bottom: Difference with the time obtained from the MoM, $T_{\max} - T_{\max,\text{MoM}}$.

a point on the scatterer(s) and $\boldsymbol{r}_1 = (x, z_1 = z)$ those of the transmitter. The polarization is vertical or TM (transverse magnetic). The scatterer surfaces are sampled with a number of points per wavelength $\lambda_0$ (in free space) equal to 20. The top surface length $L = 4$ m and it is centered on the object of depth $d$.

On the left, Fig. 3 shows the geometry and on the right, Fig. 3 plots the B-scan versus $(x_2 = x + d, t)$ computed from the MoM. In addition, the blue-dashed curve plots the points for which the strength is maximum for a given $x_2$. Fig. 4 plots the time $T_{\max} = w(x_2)$, giving the maximum of the scattered field versus $x_2$. In the legend, the labels mean:

- "M1": $T_{\max}$ is computed from equations (6), (4), (7) and (8) (no approximation).
- "M1+App": $T_{\max}$ is obtained from equations (6), (9) (approximation on the calculations of $(x_1', x_2')$), (7) and (8).
- "M1+App+Hyp": $T_{\max}$ is obtained from equation (14) (hyperbolic fitting), in which approximations (9), (13) and (15) are used. $T_{\max} > 0$ is expressed as

$$T_{\max} = -t_0 + b\sqrt{1 + x^2/a^2}, \; t_0 = 2R/v. \qquad (18)$$

- The same terminology is used for M2.
- "MoM": $T_{\max}$ is calculated from the MoM.

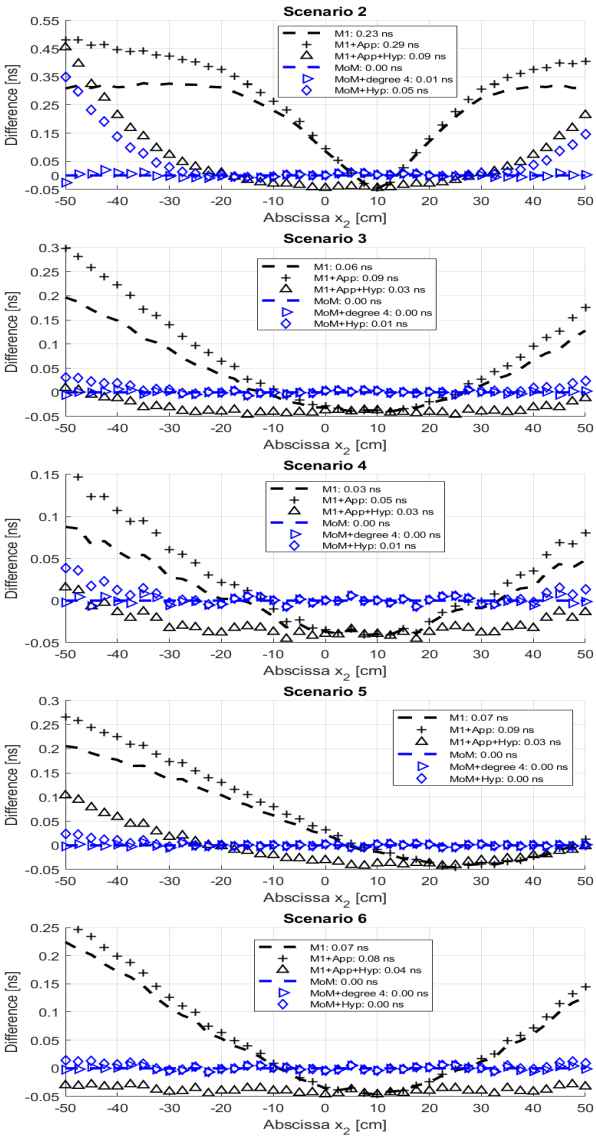


Fig. 5. $T_{\max}$ giving the maximum of the scattered field versus $x_2$. The scenario parameters are listed in Table I.

- "MoM+degree of 4": $T_{\max}$ is calculated from the MoM and it is fitted by a polynomial function of degree 4.
- "MoM+Hyp": $T_{\max}$ is calculated from the MoM and it is fitted by a hyperbola by applying the following algorithm. From equation (18), a Talyor series expansion up to the order 3 near $x = 0$ leads to

$$\begin{cases} T_{\max} \approx \alpha_0 - \alpha_1 x + \alpha_2 x^2 + \alpha_3 x^3 \\ \alpha_0 = -t_0 + ub/a, \quad \alpha_1 = bx_0/(au) \\ \alpha_2 = (ab)/(2u^3), \quad \alpha_3 = (abx_0)/(2u^5) \end{cases}, \qquad (19)$$

where $u = \sqrt{R^2 + x_0^2}$. The coefficients $\{\alpha_i\}$ can also be computed numerically from a regression of a polynomial function of fourth degree. Knowing $\{\alpha_0, \alpha_1, \alpha_2, \alpha_3\}$, from the above equation, the parameters $\{a, b, x_0, t_0\}$ are

$$\begin{cases} a = (\alpha_2^2/\alpha)\sqrt{2\alpha_1/\alpha_3} & b = (\alpha_1\alpha_2^2/\alpha_3)\sqrt{2/\alpha} \\ x_0 = (\alpha_1\alpha_2)/\alpha & t_0 = (\alpha_1\alpha_2 - \alpha_0\alpha_3)/\alpha_3 \end{cases}, \qquad (20)$$

where $\alpha = \alpha_1\alpha_3 + 2\alpha_2^2$.

To quantify the relevance of the fit, in the legend, the last number $\overline{\Delta t}$ gives the mean value of $|T_{\max} - T_{\max,\mathrm{MoM}}|$ over $x_2$. The simulation parameters are listed in Table I. The integer $i = 1$ stands for the reference scenario 1, and for $i \in [2; 6]$, only the value in bold face changes. In Table II, the time $-t_0 + b$ (evaluated at $x_2 = x_0$, hyperbola apex) and the slope $b/a$ are given for the MoM and M1. In addition, $\overline{\Delta_{x_0}}$ and $\overline{\Delta_{z_0}}$ are the mean values of $|x_{0,\mathrm{M}_1} - x_{0,\mathrm{M}_2}|$ and $|z_{0,\mathrm{M}_1} - z_{0,\mathrm{M}_2}|$ (equations (8) and (10) for M1 and M2, respectively) over $x_2$, respectively. Fig. 5 plots $T_{\max}$ for different values of $z$, $R$ $d$, $\delta$ and $\epsilon_r$ (see Table I).

In Fig. 4, the time computed from M2 are nearly the same as that obtained from M1 (the results overlaps). As shown in Table II, this comes from the fact that $(x_0, z_0)$ (in Fig. 2, coordinates of the point $M_0$ on the cylinder) are very similar for M1 and M2, since the values of $(\overline{\Delta_{x_0}}, \overline{\Delta_{z_0}})$ are very small in comparison to the cylinder radius. In Fig. 5, the results computed with method M2 are not depicted because they well match with those obtained from the method M1. This statement is in agreement with the numerical values of $(\overline{\Delta_{x_0}}, \overline{\Delta_{z_0}})$ listed in Table II, which are much smaller than the cylinder radius. In Fig. 2, this shows that the mid-point approach to calculate $x'$ is a good approximation.

As we can see in Figs. 4 and 5, both for M1 and MoM, the fitting by a hyperbola gives satisfactory results, except for scenario 2. A possible explanation is that M1 is based on the ray approach, not accounting for possible near-field effects when the receiver-transmitter is near to the top surface. For the MoM, the times computed from the fit by a polynomial function match well with those without fit. In comparison to the MoM, the M1 times (without approximation) are under-estimated and the difference decreases as $|x_2|$ increases. The deviation between "M1" and "M1+App" is weak, showing that equation (9) is a good approximation and avoid to numerically solve equation (4) of fourth degree. Table I shows that the hyperbola slope $b/a$ determined from MoM and M1 are very similar. As the radius $R$ increases, the ratio $a/b$ remains nearly constant and as the receiver height $z$ decreases, the slope increases. From equation (15), one shows

$$\frac{b}{a} \approx \frac{2}{v}\left\{1 - \frac{\delta^2(zH - d^2)}{4H(d+z)^3} - \frac{uz}{d+z}\left[1 - \frac{u(d+2z)}{2(d+z)}\right]\right\}. \tag{21}$$

The above expression clearly shows that both the horizontal offset $\delta$ and the refraction index $n = u + 1$ modified the slope $b/a$.

To reproduce real data, for all the scenarii, a Gaussian white noise is added to the MoM A-scan by considering a noise signal ratio equals 10 dB. The numerical results showed that the maximum deviation of $T_{\max}$ from those obtained without noise does not exceed 0.06 ns. This value is the same order of $\overline{\Delta t}$ given in the legends of Figs. 4 and 5.

## IV. Conclusion

In this paper, for a coupled-air bistatic configuration, the round trip time $t = w(x_2)$ from a buried circular cylinder in a homogeneous single layer medium is derived from three methods. The first two ones, "M1" and "M2", are analytical and based on a ray approach and the third one, is numerical and based on the full-wave MoM, the reference solution. M1 published in literature, assumes that the ray coming from the cylinder cut the abscissa axis in the middle of the transmitter and receiver locations. The new method M2 is based on a more physical principle, which states that the reflected ray direction is the bisector of the angle between the [Transmitter-A point on the cylinder-Receiver] (specular reflection).

The numerical results show that M1 and M2 give nearly identical results, validating the method M1. For method M1, to approximate $w$ by a hyperbola, a Taylor series expansions are applied up to the second order over $x = 0$ and $\delta = 0$. Comparisons of M1 with MoM reveal that M1 predicts satisfactory results and $w$ computed from M1 can be fitted by a hyperbola with a satisfactory agreement. This means that the simple closed-from expressions (13), (14), (15) and (21) can be applied to solve the forward problem avoiding to use the more complicated equation (6). With the MoM, the function $w$ matches well with that computed by a polynomial regression of fourth degree whereas the fitting by a hyperbola is satisfactory.

## References


[1] W. Li, H. Zhou, and X. Wan, "Generalized Hough transform and ANN for subsurface cylindrical object location and parameters inversion from GPR data." Shanghaji, China: Proc. of 14th International Conference on Ground Penetrating Radar, Jun. 2012, pp. 285–89.

[2] F. C. J. Sham and W. L. W. Lai, "A new algorithm for more accurate estimation of wave propagation velocity by common-offset survey method," in *International Symposium Non-Destructive Testing in Civil Engineering (NDT-CE)*, Sep. 2015.

[3] L. Mertens, R. Persico, L. Matera, and S. Lambot, "Automated detection of reflection hyperbolas in complex GPR images with no a priori knowledge on the medium," *IEEE Transactions on Geoscience and Remote Sensing*, vol. 54, no. 1, pp. 580–96, 2016.

[4] F. Xie, W. L. Lai Wallace, , and X. Drobert, "GPR-based depth measurement of buried objects based on constrained least-square (CLS) fitting method of reflections," *Measurement*, vol. 168, Jan. 2021.

[5] R. M. Jaufer, I. Ihamouten, Y. Goyat, S. S. Todkar, D. Guilbert, A. Assaf, and X. Drobert, "A preliminary numerical study to compare the physical method and machine learning methods applied to gpr data for underground utility network characterization," *Remote Sensing*, vol. 14, 2022.

[6] T. Wunderlich, D. Wilken, B. S. Majchczack, M. Segschneider, and W. Rabbel, "Hyperbola detection with retinanet and comparisonof hyperbola fitting methods in GPR data from an archaeological site," *Remote Sens.*, vol. 12, no. 15, pp. 1–22, 2022.

[7] F. Giannakis, I. Zhou, C. Warren, and A. Giannopoulos, "On the limitations of hyperbola fitting for estimating the radius of cylindrical targets in nondestructive testing and utility detection," *IEEE Geos. Rem. Sensing Letters*, vol. 19, 2022.

[8] R. Persico, G. Leucci, L. Matera, L. De Giorgi, F. Soldovieri, A. Cataldo, G. Cannazza, and E. De Benedetto, "Effect of the height of the observation line on the diffraction curve in gpr prospecting, near surface geophysics," *Near Surface Geophysics*, vol. 13, no. 3, pp. 243–252, 2014.

[9] C. Bourlier, N. Pinel, and G. Kubické, *Method of moments for 2D scattering problems. Basic concepts ans applications*, ser. Focus Series. London, UK: ISTE Ltd, John Wiley & Sons, Inc., 2013.

[10] C. Bourlier, "Rough layer scattering filled by elliptical cylinders from the Method of Moments combined with the Characteristic Basis Function method and the Kirchoff approximation," *Journal of the Optical Society of America A*, vol. 38, no. 10, pp. 1581–1593, 2021.